forests

MDPI

Article

An Innovative Approach to Surface Deformation Estimation in Forest Road and Trail Networks Using Unmanned Aerial Vehicle Real-Time Kinematic-Derived Data for Monitoring and Maintenance

Evangelia Siafali [1] and Petros A. Tsioras [2,*]

[1] Laboratory of Forest Engineering and Topography, School of Forestry and Natural Environment, Aristotle University of Thessaloniki, 541 24 Thessaloniki, Greece; esiafali@for.auth.gr
[2] Laboratory of Forest Utilization, School of Forestry and Natural Environment, Aristotle University of Thessaloniki, 541 24 Thessaloniki, Greece
* Correspondence: ptsioras@for.auth.gr

Abstract: The significant increase in hiking, wood extraction, and transportation activities exerts a notable impact on the environmental balance along trails and forest roads in the form of soil degradation. The aim of this study was to develop a Deformation Classification Model for the surface of a multi-use trail, as well as to calculate sediment deposition and generate a flood hazard map in a partially forested region. The eBee X mapping Unmanned Aerial Vehicle (UAV) equipped with the senseFly S.O.D.A. 3D camera and Real-Time Kinematic (RTK) technology flew over the study area of 149 ha in Northern Greece at an altitude of 120 m and achieved a high spatial resolution of 2.6 cm. The specific constellation of fixed-wing equipment makes the use of ground control points obsolete, compared to previous, in most cases polycopter-based, terrain deformation research. Employing the same methodology, two distinct classifications were applied, utilizing the Digital Surface Model (DSM) and Digital Elevation Model (DEM) for analysis. The Geolocation Errors and Statistics for Bundle Block Adjustment exhibited a high level of accuracy in the model, with the mean values for each of the three directions (X, Y, Z) being 0.000023 m, −0.000044 m, and 0.000177 m, respectively. The standard deviation of the error in each direction was 0.022535 m, 0.019567 m, and 0.020261 m, respectively. In addition, the Root Mean Square (RMS) error was estimated to be 0.022535 m, 0.019567 m, and 0.020262 m, respectively. A total of 20 and 30 altitude categories were defined at a 4 cm spatial resolution, each assigned specific ranges of values, respectively. The area of each altitude category was quantified in square meters (m^2), while the volume of each category was measured in cubic meters (m^3). The development of a Deformation Classification Model for the deck of a trail or forest road, coupled with the computation of earthworks and the generation of a flood hazards map, represents an efficient approach that can provide valuable support to forest managers during the planning phase or maintenance activities of hiking trails and forest roads.

Keywords: forest management; terrain analysis; environmental impact assessment; erosion model; earthworks; timber extraction; GPS; 3D Model; photogrammetry

check for updates

Citation: Siafali, E.; Tsioras, P.A. An Innovative Approach to Surface Deformation Estimation in Forest Road and Trail Networks Using Unmanned Aerial Vehicle Real-Time Kinematic-Derived Data for Monitoring and Maintenance. *Forests* **2024**, *15*, 212. https://doi.org/10.3390/f15010212

Academic Editors: Sang-Kyun Han, Heesung Woo and Jae-Heun Oh

Received: 7 December 2023
Revised: 17 January 2024
Accepted: 18 January 2024
Published: 21 January 2024

1. Introduction

Forest roads play a vital role in facilitating access to and management and exploitation of forested areas, aiding in the efficient and cost-effective transportation of timber from the logging site to areas of concentration and processing [1–7], and also in supporting the development of mountainous regions. Therefore, the proper construction and maintenance of forest roads is imperative for ensuring smooth vehicular movement [8]. Trails also serve as primary gateways to natural environments. The demand for pleasant environments is increasing due to increased leisure time and greater standards of living, with growing urbanization [9–13] giving considerable rise to widely favored activities such as hiking, jogging and mountain biking that are facilitated by the utilization of trails [9,10,14–18]. Trails are also used for traditional purposes, such as forest operations. The appropriate design and construction of a trail according to specific technical specifications aims to save resources and minimize maintenance and management issues [19]. Studies demonstrate that a trail's design—its position and alignment with topography and soils—is the most significant variable in long-term sustainability [20–22]. Sustainable hiking trails are created, constructed, and managed to meet intended uses and seasons, providing high-quality visitor experiences while maintaining trail infrastructure and natural resources.

The sensitivity of forest roads and trails can be impacted by a range of natural elements, including soil slope, soil characteristics, altitude, exposure, precipitation, vegetation composition, and canopy cover [23–34]. A broad range of studies have tried to explore the consequences linked to the utilization of collective activities centered around recreational trails, such as hiking, including comparisons between different activities [23,35,36] and varying levels of use [37–42]. From a conservation standpoint, the primary environmental concern lies in soil erosion due to its long-term or irreversible nature without effective management. The degradation of forest road networks and trails, particularly the erosion of soil, is a complex phenomenon with multiple components [42]. Skid trails locally increase soil compaction and forestry activities may cause sedimentation of surface water if best management practices are not implemented during forest operations [43,44]. The harvesting method, number of machine passes, soil tilt, type, texture, and water content, among others, affect soil compression and rutting during mechanized logging as forest operations can have a significant impact on the physical and chemical qualities of soil [45–49]. Road rills accelerate sediment erosion. Skidding and forwarding are the two most prevalent methods used for extracting materials from the ground's surface. Skidding involves the act of pulling the wood along the ground, whereas forwarding entails transporting the timber on a loading deck. The sustainability of a certain extraction technology is determined not only by its cost-effectiveness but also by its capacity to minimize disruption to forest soil and natural ecosystems [50,51]. Latterini et al. (2024) indicate that skidding results in a higher amount of soil displacement compared to advancing, whereas elevated soil rutting follows, increasing forwarding activity. Best management measures can reduce sediment erosion, but determining which factors most affect forest road rill development is crucial to implement them efficiently [3]. Despite this requirement, the literature on forest road rill development is limited.

Accurate spatial information on forest road network elements is important for forest management [52] and harvesting operations [53]. Maintenance of a forest road network plays an important part in ensuring its effective management [54] and monitoring road surfaces is a key element of transportation infrastructure. The need for accurate topographic estimations can be covered by Terrestrial Laser Scanning (TLS) and the utilization of UAVs in forested areas [19]. Airborne and terrestrial laser scanning, as well as close-range photogrammetry, are frequently used techniques for the purpose of achieving highly detailed land surface mapping [55]. The successful implementation of these techniques involves the development of a comprehensive mapping strategy in order to achieve optimal visibility across every area [56].

Unmanned Aerial Vehicles (UAVs) have been proven to be highly effective equipment for acquiring reliable data in forested areas, combining simplicity and less need for resources in terms of manpower, equipment, time, and cost [57]. This winning combination justifies the research that has been undertaken with regard to possible implementations of UAVs equipped with cameras and sensors in forest engineering. Their capability to generate high-resolution images in an accurate and cost-efficient manner facilitates comprehensive inspection and monitoring processes [2,58–60]. Due to their vertical take-off and landing, lack of sensitivity to different environments, high mobility and stability, and ease of operation, quadripellers are more durable than their predecessors and produce high-quality results that allow researchers to manage reliability and accuracy [61–63]. Furthermore, the use of UAV-mounted GNSS–real-time kinematic (GNSS–RTK) receivers has increased because they provide higher accuracy in the measurement of the UAV camera position [64] and minimize or even eliminate the need for ground control points (GCPs) [65].

UAV photogrammetry, which refers to the combination of a UAV with a Light Detection and Ranging (LiDAR) sensor, has advanced rapidly over the last decade, enabling three-dimensional modeling for the protection and management of natural ecosystems, among others [57]. LiDAR sensors have a high resolution and accuracy when measuring objects [66] and represent a promising technology for road maintenance in the near future [67]. Zeybek and Bicici [68] have shown that LiDAR sensors can detect deformations on the road surface. This 3D sensor technology will revolutionize measurement methods, offering high-density data and visualizations for small-scale projects. Considering the integration of LiDAR sensors in smartphones, they might be a cost-effective remote-viewing alternative in the near future [54], facilitating quick and accurate data collection [69] and, most importantly, easy mapping and inspection of forest roads lacking GNSS coverage [54,69–71]. Nakagomi et al. [66] introduced a novel approach for road monitoring by leveraging Light Detection and Ranging Simultaneous Localization and Mapping (LiDAR-SLAM) and a convolutional neural network (U-Net) architecture. LiDAR-SLAM demonstrates high accuracy in estimating road form in response to environmental variations, whilst the U-NET architecture proves to be useful in estimating pavement conditions. Tan and Li [4] proposed a cost-effective, efficient, and automated technique for detecting road surface damage using UAV photogrammetry images. First, they used UAV images to generate road 3D models from which they extracted the pavement surface from irrelevant surroundings by using a region-expanding algorithm. The study indicated the potential of the specific technique in accurately identifying road distress locations with a centimeter-level height/depth inaccuracy. Hrůza et al. [72] tried to assess the feasibility and accuracy of various 3D imaging techniques in detecting damage to the asphalt wearing course of forest roads in an effort to simplify and speed up the process of damage detection. In their study, four different methodologies, close-range photogrammetry, terrestrial laser scanning, mobile laser scanning, and airborne laser scanning, were compared, with the first two performing best.

The objective of this study is to develop a novel approach that identifies classes of surface deformation on a multi-use forest trail using a fixed-wing UAV equipped with a LiDAR sensor and RTK technology, compared to previous research where polycopters have been used. By utilizing this specific equipment, we aspire that the proposed methodology is characterized by faster implementation and high-accuracy data collection for large-scale projects. The collected data can be utilized to improve the terrain's condition, streamline its administration, and facilitate the implementation of technical measures and interventions in specific segments. The presented method can be also implemented to forest road networks. This novel approach aims to maximize the benefits and minimize costs, while minimizing the degradation of the surrounding natural environment.

2. Materials and Methods

2.1. Study Area

The study area (Figure 1) is located to the southeast (SE) side of the Kassandra peninsula, Halkidiki, approximately 100 km from the metropolitan center of Thessaloniki, and covers an area of 149 ha (N 40.015460 E 23.48901 to N 40.00150 E 23.51992). This particular area was chosen as it is the first region in Halkidiki to attain a national-level certification for its network of paths. Additionally, the study area is managed by the Greek Forestry Service, adheres to the specifications of the European Ramblers' Association, and has served as a research area for a PhD study [19]. More specifically, we investigated a circular path, comprising segments of both a forest road and a multi-purpose forest trail, for pavement deformations (hereafter it will be referred to as "trail"). The examined trail spans a total length of 3200 m, with an elevation ranging from 154 m to 233 m. The trail traverses established agroforestry systems. The Mavrobara lake is positioned around 2100 m away from the starting point of the route and it lends its name to the region (Figure 2).

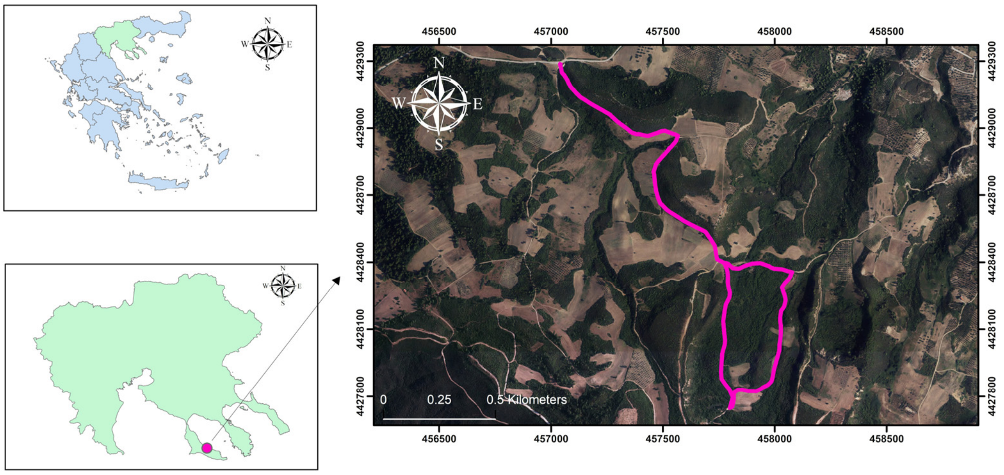

Figure 1. The study area (Source: Siafali Evangelia 2023).

(**a**) (**b**) (**c**) (**d**)

Figure 2. Photos of the study area: (**a**,**b**) aspects of the examined trail, (**c**) typical landscape of the study area, and (**d**) lake Mavrobara (Source: Siafali Evangelia 2023).

2.1.1. Vegetation of the Study Area

The Municipality of Kassandra has a total of 172 taxa, including species and subspecies which are spatially distributed within the forests of the peninsula. The region includes a variety of therophytes and semi cryptophytes species. This information also serves to ecologically describe the climate of the research location. From a phyto-sociological perspective, the region is classified within the broad-leaved (*Quercetalia ilicis*) zone, more precisely within the habitat where *Pinetum halepensis* thrives, interspersed with the presence of *Oleo lentiscetum* vegetation [73].

2.1.2. Flood Risk Management Conditions

The absence of major rivers in Halkidiki contributes to the exceptional clarity of its seas. The hydrographic network of mountains exhibits a branched pattern, with the possibility of rectangular formations resulting from tectonic forces [73]. According to the Flood Risk Management Plan of the Central Macedonia Water Park (GR10) River Basin Reservoirs, the Mavrobara region is situated inside the GR10RAK0003 zone and has a total area of 211 km^2. The historical flood record indicates that the research area does not exhibit any significant danger of flooding. Within the Mavrobara region, there is an established network of streams originating from the surrounding forest. These streams are characterized by their limited water flow during the summer season, with a small number of them maintaining a consistent water supply. The small length of these watercourses, along with the presence of forest cover, serves as a barrier to flood phenomena.

2.2. Equipment

To conduct the research, the following equipment and software were used (Figure 3): (i) the SenseFly eBeeX, a fixed-wing Unmanned Aerial Vehicle (UAV) (AgEagle Aerial Systems, Wichita Inc., KS, USA) that can fly continuously for up to 90 min and can cover an area of 500 ha, with an absolute accuracy of 1.5 cm (Table 1), (ii) the S.O.D.A. 3D drone photogrammetry camera (AgEagle Aerial Systems Inc., Wichita, KS, USA) that captures three images (2 oblique, 1 nadir) every flight, resulting in a broader field of view; it is optimized for fast, reliable image processing using PIX4Dmapper, (iii) the eMotion flight planning software version 3 (AgEagle Aerial Systems Inc., Wichita, KS, USA), (iv) PIX4Dmapper version 4.6.4 (Pix4D Inc., Denver, CO, USA), a photogrammetry program for professional drone mapping, and (v) ArcGIS Desktop 10.8.1 (ESRI Inc., Redlands, CA, USA), an integrated suite of Geographic Information Systems software that facilitates map creation, spatial analysis, and data management.

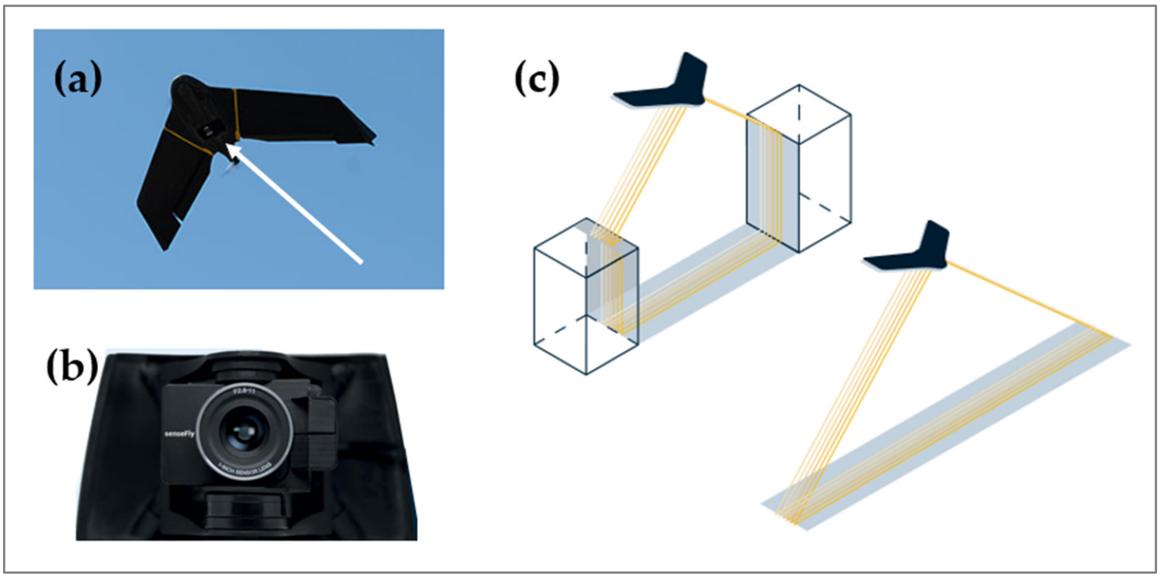

Figure 3. Study equipment: (**a**) Sensefly eBee X UAV with the white arrow indicating the position of photogrammetry cameras, (**b**) the S.O.D.A. 3D drone photogrammetry camera, and (**c**) graphical presentation of data collection with the specific equipment (AgEagle Aerial Systems, Wichita, KA, USA).

Table 1. SenseFly eBeeX specifications and overview of performance metrics and capabilities.

Specification	Value
Cruise speed	11–30 m/s (40–110 km/h)
Max. wind resistance	Up to 12.8 m/s (46 km/h)
Landing type	Automatic linear landing (5 m accuracy in 35° angle cone)
Service temperature *	5° to 104 °F (−15° to 40 °C)
Humidity	Light rain resistance
Ground avoidance	Yes–LiDAR (range 120 m)
Ground resolution	Down to 1.5 cm
Max. flight time	90 min
Coverage at 400 ft/120 m	220 ha to 500 ha
Linear coverage	Up to 27.7 km out and back

* Working above 35 °C requires protecting the drone from the sun while on the ground.

2.3. UAV Survey and Image Collection

A comprehensive analysis was undertaken in the Mavrobara region, which covers the trail of interest. The analysis involved generating an orthomosaic, the Digital Surface Model (DSM), and the Digital Elevation Model (DEM), along with the development of a trail surface deformation index. Additionally, a map demonstrating the risk of flooding phenomena in the area was generated, accompanied by an index assessing deformations of the trail surface.

In May 2021, the flight tracks were systematically arranged in a grid pattern at an elevation of 120 m, utilizing the eBee X. The duration of the flight for the area was approximately 45 min, with a low wind speed and perfect weather conditions. The aerial images were configured with a frontal overlap of 85% and a side overlap of 75% in order to enhance the accuracy of the resulting outputs. The availability of real-time kinematic (RTK) solutions was decisive in foregoing the placement of Fixed GCP markers, given the time-consuming nature of GCP deployment. An enhanced Shuttle Radar Topography Mission (SRTM) DSM is incorporated within the software. The software computes the Ground Sampling Distance to be 2.6 cm at an altitude of 120 m. However, due to an altitude variation in the vicinity in which the UAV operated, it ascended further, thereby resulting in a spatial resolution of 4 cm, as calculated by the model.

Following the completion of the flight, the data were subsequently inserted into the Pix4DMapper photogrammetry software version 4.6.4., which enables the orientation and combination of the aerial images (Figure 4). The image processing procedure involved key steps, such as picture alignment for initial processing, dense point cloud generation for point cloud and mesh creation, as well as DSM, DEM, and orthomosaic creation. During the final stage, several road distresses were identified and quantified based on the orthomosaic and DSM data using the ArcGIS Desktop Software. In conclusion, we generated a set of 3D point clouds and a georeferenced orthomosaic map with a spatial resolution of 4 cm/px in the Greek Reference System EGSA87.

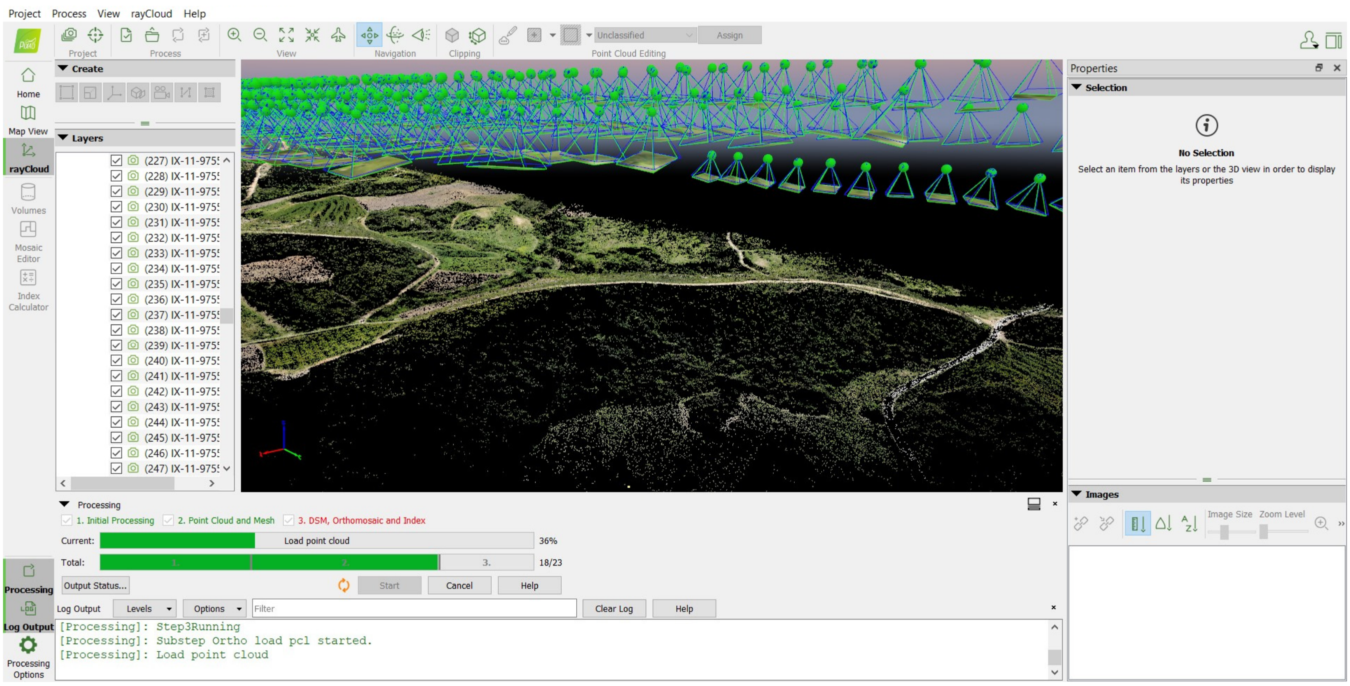

Figure 4. Processing stages in the Pix4D Mapper software.

2.4. Generation of Trail Surface Deformation Index

The primary goal of this study was to classify deformations occurring along the surface of the trail. Our objective was to improve the condition of the trail by facilitating more accurate management and providing measurement data for the implementation of technical structures and interventions in specific segments of the trail. In order to finalize the generation of deformation classes for the road surface, the following elements were implemented: (i) an orthomosaic map georeferenced to the Greek Reference System EGSA87 provided a geospatially accurate representation of the study area, (ii) a DEM that was employed to capture the bare-earth surface, (iii) a DSM with a spatial resolution of 4 cm/px that served as a presentation of both terrain and above-ground features, and (iv) the polyline shapefile of the trail that included its spatial attributes. These data sets were imported into ESRI's ArcMap 10.8 software to proceed to further analysis and processing.

The data collected by the Ebee X flight were imported into the Pix4D Mapper photogrammetric software. The specific software was used to generate the DSM and DEM. The generated products were then imported into the ArcGIS 10.8 software. The next process in the DSM generation workflow was the process of converting the trail into a digital format by generating a new polygon shapefile using the Editing tool. The option to create a buffer zone was not preferred because of the inaccuracies in GPS-traced polygon generation along the trail, especially in forested settings where GPS accuracy was low. The polygon representing the trail was extracted using the Clip tool in the Raster Management menu. The raster, derived from the application of box classification to the DSM clip of the trail, was subsequently utilized in the Neighborhood tool within Spatial Analyst. Using the Focal Statistics tool, we defined three box ranges in pixel sizes: 3 cm × 3 cm, 4 cm × 4 cm, and 5 cm × 5 cm, respectively. The "RANGE" option was used, which is not a physical unit but rather a continuum of values that determines the level of smoothness observed on the trail pavement. The next phase involved the reclassification of the box ranges for each pixel size into 20 distinct classes. Following this, the files Reclass_3×3, Reclass_4×4, and Reclass_5×5 and the color palette for the 20 classes were chosen from the Symbology menu. The most effective range for detecting variations based on the topography of the trail and its surroundings was Reclass_4×4, which has a box range of 4 cm × 4 cm. The initial group of 10 classes was created, with each class having a width of 1 cm, and this was succeeded by an additional 9 classes, each with a width of 5 cm per class. The 20th class had values exceeding 55 cm, which were assigned to various objects such as trees, buildings, pillars, and steep slopes. These values were only taken into account for certain maintenance-related tasks.

Following the classification of the elevational groups corresponding to the distortions seen on the route, further steps involved the calculation of the surface area associated with each class, as well as the calculation of the amount of material to be excavated and deposited for the trail. A reclassification of the raster data was conducted, resulting in the creation of deformation classes. These classes were based on altitude classifications above sea level. With this method, it is possible to identify regions exhibiting deformations of up to 55 cm initially. These areas can be rectified through technical interventions and by removing excess material from the trail surface. Furthermore, by carefully examining abrupt variations in the terrain and conducting empirical observations in the field, combined with the utilization of an orthomosaic as a background for analysis, it is feasible to ascertain that the elevated values within the raster range are attributable to the presence of trees, cables, and buildings close to the trail.

The area of each class in the attribute table was calculated through conducting calculations, as described in Equation (1). This involved multiplying the number of pixels corresponding to each class by the size of the pixel, as specified in Equation (2).

$$\text{Area\_cm}^2 = \text{pixel count} \times \text{cell size} \tag{1}$$

where cell size = 16 cm^2 (cell dimensions: 4 cm × 4 cm)

$$\text{Area of each class} = \text{Number of pixels of each class} \times \text{area of pixel} \tag{2}$$

To determine the earthworks volume for each category, a mask was created to generate separate DEMs for each class. The Reclass_4×4 file underwent reclassification, assigning a value of 1 to the desired volume values and 0 to the excluded values. This process led to the generation of a DSM for each individual class. Then, the mean heights inside the DEM were computed using Equation (3). Furthermore, Equation (4) was employed to multiply the resulting elevation by the corresponding area of each class.

To calculate the average elevation of the trail, the DSM was imported into ArcMap. The Focal Statistics tool was utilized, specifically selecting the "MEAN" option, with a pixel range of 100 × 100 (equivalent to 4 m × 4 m, approximately the width of the trail). Later, we performed the subtraction operation between the DEM representing the forest trail and the DSM, as indicated by Equation (3).

$$\mathrm{Dif}_{\mathrm{DEM}} = \mathrm{DSM}_{\mathrm{trail}} - \mathrm{DEM}_{\mathrm{trail}} \quad (3)$$

$$\text{Average elevation} \times \text{pixel area} \times 100 \quad (4)$$

$\mathrm{Dif}_{\mathrm{DEM}}$ was reclassed into two cut and fill classes:

- Class 1 for positive values (cut: remove volume of material from the surface);
- Class 2 for negative values (fill: add material to the surface).

A similar approach was utilized for the generation of the 30 classes, this time based on the DEM, aiming for a more accurate visualization of the surface deformations.

2.5. Generation of a Flood-Risk Map

To create the flood hazard model for the surveyed area, the DEM acquired through surveying with the eBeeX UAV drone, together with the shapefile delineating the borders of the area, were imported into ArcMap 10.8. The Strahler method was employed for the assignment of stream order branches within the hydrographic network [74]. Data processing was conducted utilizing the Hydrology tool within the Spatial Analyst Tools. The processing steps included: filling soil depressions, determining flow direction, estimating watershed flow accumulation, delineating the hydrographic network, segmenting branches, and assigning stream order numbers. Additionally, the identification and mapping of potential flood-prone areas was also included in the data processing workflow. This classification process is informed by various data inputs, including historical precipitation data, soil composition data, slope data of the area, and data on land uses and forms of cover.

3. Results

3.1. Camera Sensor Accuracy

The ability of a camera sensor to capture a greater amount of light information within a given time period is proportional to its size. Furthermore, noise is the phenomenon of randomized fluctuations in the brightness or color information in pictures, typically arising from electrical noise. A critical aspect of internal camera parameters is maintaining a principal point size approximately half that of the camera, while ensuring that the radial distortion values (R1, R2, and R3) and the tangential distortion values (T1 and T2) remain below 1. The camera utilized exhibited excellent performance in all accuracy assessments, as summarized in Table 2.

Table 2. Internal camera accuracy assessment.

	Focal Length	**Principal Point x**	**Principal Point y**	**R1**	**R2**	**R3**	**T1**	**T2**
Initial Values	4430.420 pixel 10.633 mm	2725.000 pixel 6.540 mm	1811.670 pixel 4.348 mm	0.033	−0.209	0.315	0.000	0.000
Optimized Values	4393.184 pixel 10.544 mm	2720.287 pixel 6.529 mm	1805.932 pixel 4.334 mm	0.028	−0.196	0.297	0.000	0.001
Uncertainties (Sigma)	0.218 pixel 0.001 mm	0.118 pixel 0.000 mm	0.108 pixel 0.000 mm	0.000	0.001	0.001	0.000	0.000

Camera model: S.O.D.A._10.6_5472x3648 (RGB). Sensor Dimensions: 13.133 [mm] × 8.755 [mm].

Furthermore, it is essential to constrain the uncertainty associated with the focal length and principal point to a minimal number of pixels, while ensuring that uncertainties related to distortion parameters approach zero. In both uncertainty assessments, the S.O.D.A. 3D camera demonstrated exceptional performance.

3.2. UAV Data Accuracy Statistics

A UAV flight was conducted over the study area. The elevation of the study area ranged from 123 m to 285 m. Radiometric Correction Types involved adjustments pertaining to camera, sun irradiance, and sun angle.

The examination of the aerial images was carried out using Pix4D Mapper, resulting in the successful calibration of 460 out of a total of 461 pictures. The Bundle Block Adjustment process generated a count of 2,279,916 3D points and 5,363,247 2D points, while the generated point cloud consisted of 70,597,537 points.

Geolocation error is the difference between the original and calculated image positions in the photogrammetry software. Table 3 assesses the quality of the image geolocation by presenting information on the percentage of geolocated and calibrated images that exhibited inaccuracies in the X, Y, and Z coordinates, within predefined error ranges. There were ten predefined intervals within the range of −1.5 to 1.5 times the maximum accuracy (A_{max}) of all images. If a significant proportion of the photos exhibited errors that fell below $-1.5 \times A_{max}$ or exceeded $1.5 \times A_{max}$, it was possible that the accuracy values were not properly adjusted. Minimum Error and Maximum Error represent Geolocation Error intervals between −1.5 and 1.5 times the maximum accuracy of all images. The mean, representing the average error in each of the three directions (X, Y, Z) was 0.000023 m, −0.000044 m, and 0.000177 m, respectively. Sigma, indicating the standard deviation of the error in each direction, was 0.022535 m, 0.019567 m, and 0.020261 m, respectively. Furthermore, the Root Mean Square (RMS) error was found to be 0.022535 m, 0.019567 m, and 0.020262 m, respectively.

Table 3. Geolocation errors and statistics for Bundle Block Adjustment.

Min Error (m)	Max Error (m)	Geolocation Error (%)		
		X	Y	Z
–	0.06	−0.87	0.43	0.22
−0.06	−0.05	1.09	0.87	0.43
−0.05	−0.04	3.91	1.52	1.74
−0.04	−0.03	4.57	5.00	9.35
−0.03	−0.01	15.00	15.22	15.43
−0.01	0.00	25.22	26.52	22.61
0.00	0.01	23.04	29.13	21.30
0.01	0.03	14.57	14.35	18.70
0.03	0.04	7.83	4.13	7.83
0.04	0.05	2.39	1.52	2.17
0.05	0.06	0.43	1.09	0.22
0.06		−1.09	0.22	0.00
Mean (m)		0.000023	−0.000044	0.000177
Sigma (m)		0.022535	0.019567	0.020261
RMS Error (m)		0.022535	0.019567	0.020262

Figure 5a depicts the computed image positions with links connecting matched images. The intensity of the links serves as an indicator of the quantity of matched 2D points between the images. Bright links indicate weaker connections that require additional manual connection points or the inclusion of more images. The dark green ellipses indicate the uncertainty of the relative camera position based on the beam block fitting result. Figure 5b illustrates the number of overlapping images calculated for each pixel in the orthomosaic. Regions highlighted in red and yellow indicate low overlap, resulting in poor data production, while green areas indicate an overlap of more than 5 images for each pixel. High-quality results can be generated as long as a sufficient number of keypoint matches are available.

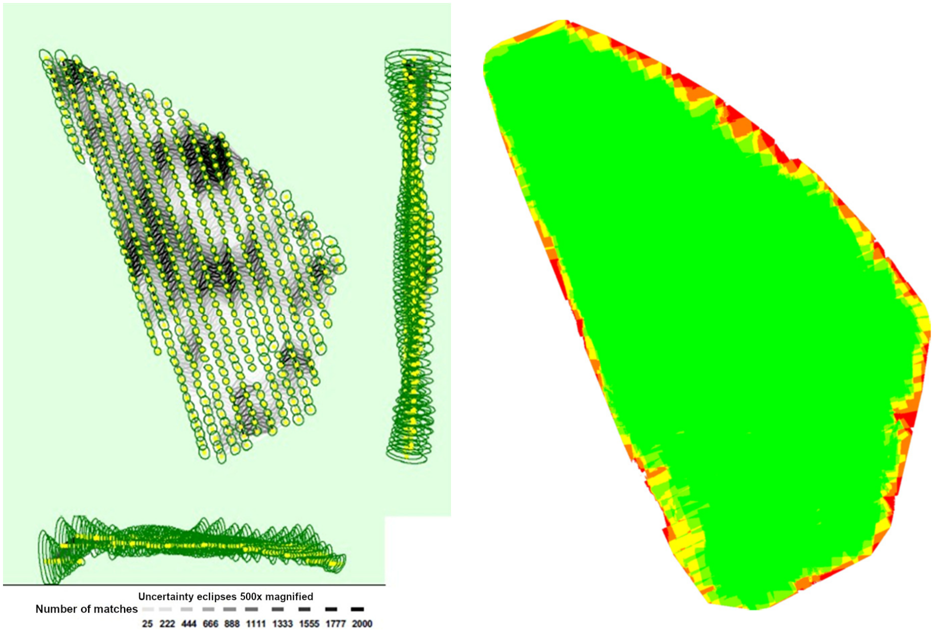

(**a**) (**b**)

Figure 5. (**a**) Two-dimensional keypoint matches and (**b**) orthomosaic overlap. Red and yellow regions indicate low overlap, while green areas represent an overlap of more than 5 images per pixel.

3.3. DEM Generation

Following the processing and analysis of the data, in the Pix4DMapper software, the orthomosaic and the corresponding sparse DSM before any densification process were developed and are depicted in Figure 6.

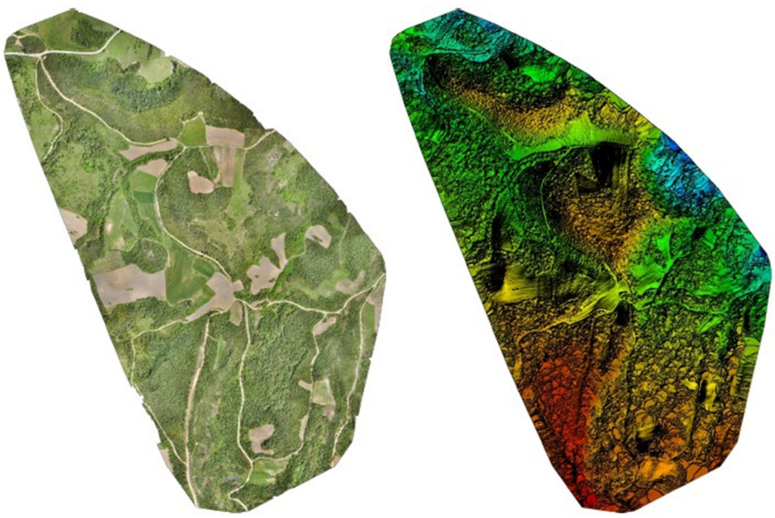

(**a**) (**b**)

Figure 6. (**a**) Orthomosaic and (**b**) the corresponding sparse Digital Surface Model (DSM) before densification (Source: Siafali Evangelia 2023).

Key aspects of the study area are presented in Figure 7. These include the DEM, the DSM, the slope map, and the aspect map.

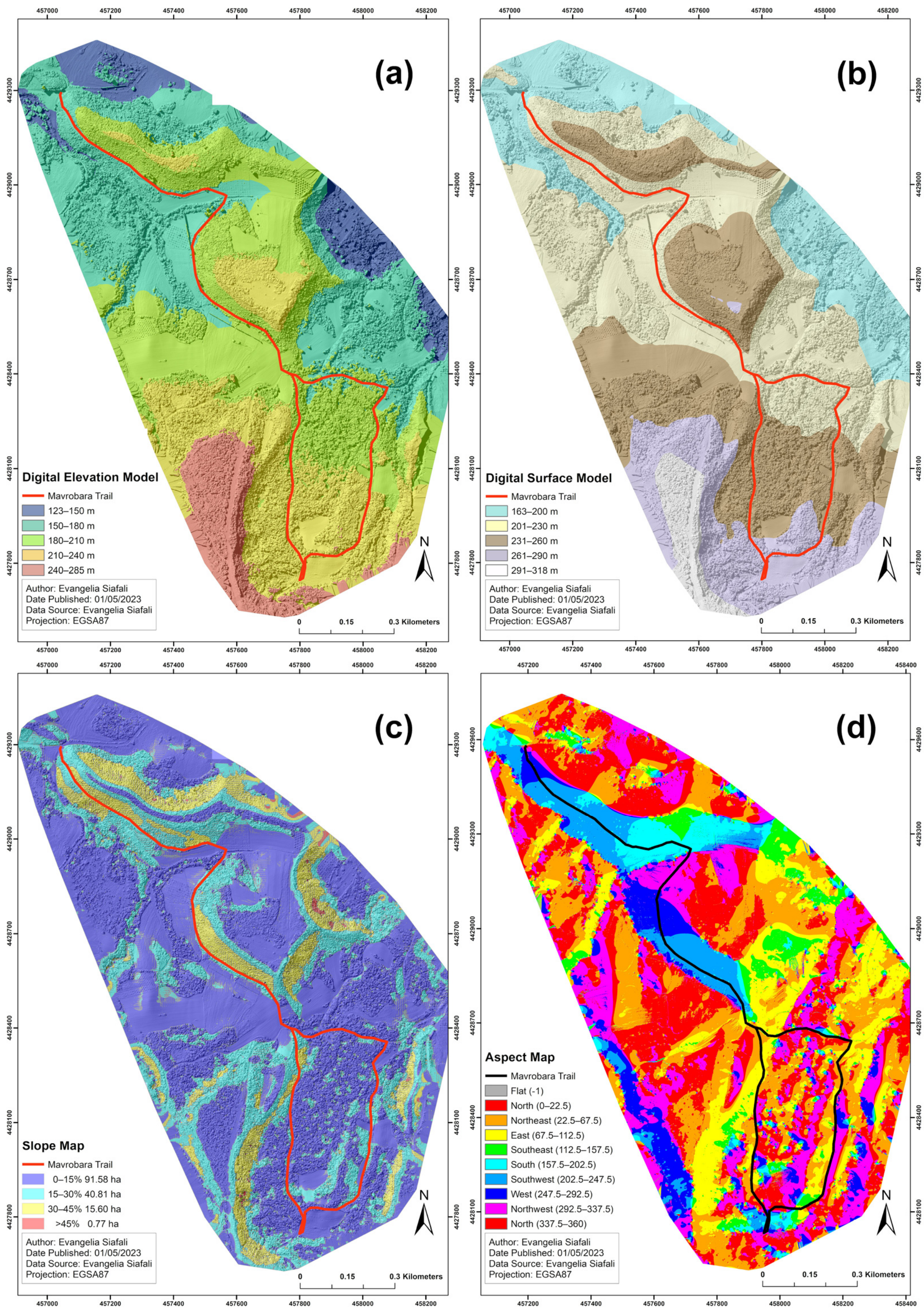

Figure 7. Key aspects of the study area: (**a**) Digital Elevation Model, (**b**) Digital Surface Model, (**c**) slope map, and (**d**) aspect map (Source: Siafali Evangelia 2023).

Figure 8 illustrates the Normalized Vegetation Index (NDVI), the aspect map of the trail, the DEM, and a slope map. These visual representations are crucial for conducting a comprehensive planning process for the installation of technical infrastructure, as well as in the management and categorization of the trail. The objective is to align with the selection criteria established by the European Ramblers' Association [75], ensuring certification at both the European and national levels; this is important as it outlines the technical specifications for the marking, marking, opening, and maintenance of hiking paths.

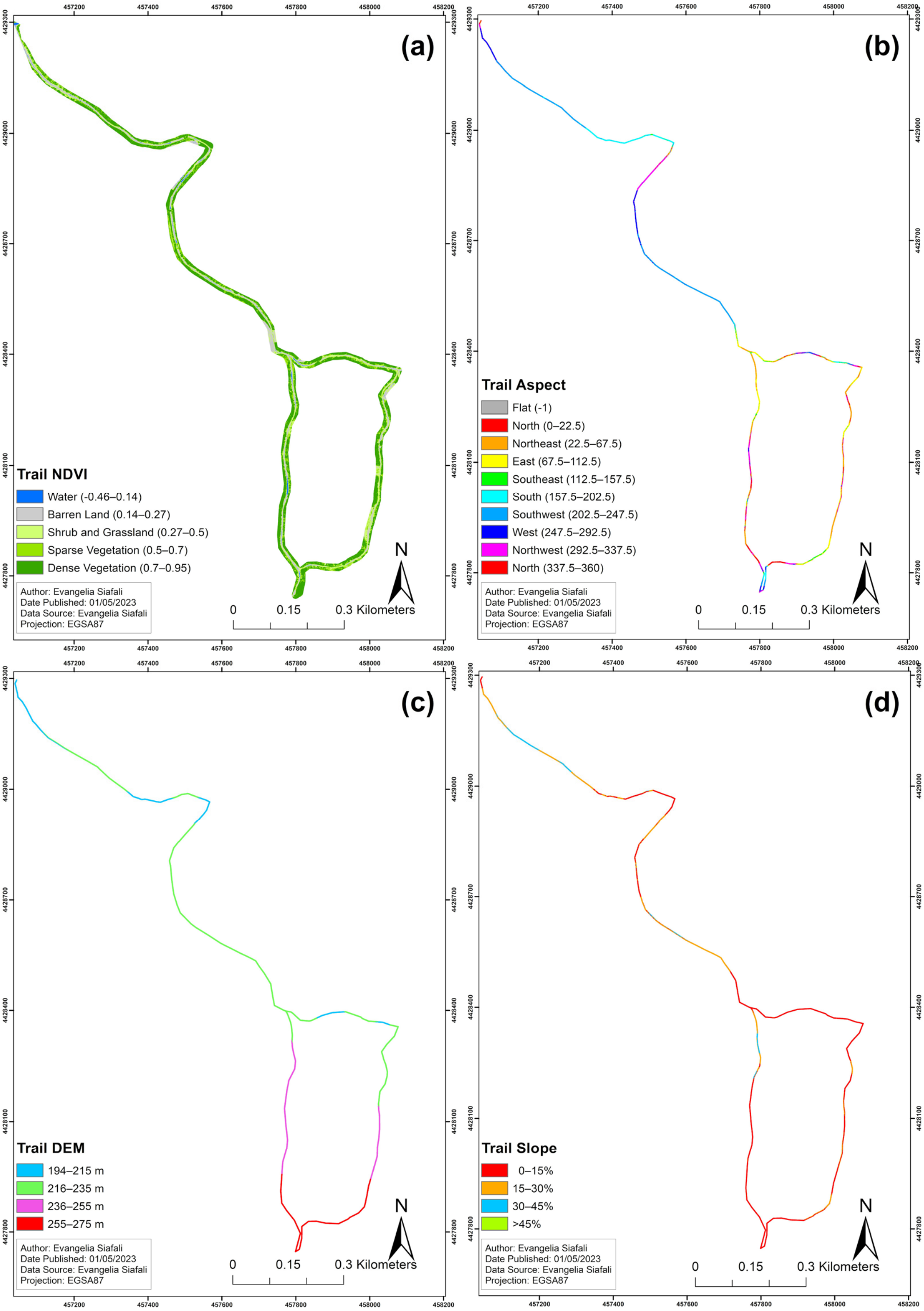

Figure 8. Maps of the examined trail: (**a**) Normalized Vegetation Index map, (**b**) aspect map, (**c**) trail DEM, and (**d**) slope map (Source: Siafali Evangelia 2023).

3.4. Trail Deformation Index

The volumetric measurements of excavation and embankment materials for the entire length of the trail, together with the classification of corresponding deformations, were based on the 3 cm × 3 cm box range, which provides the highest amount of detail. The observed differences in surface deformation between the 3 cm × 3 cm box range and the 5 cm × 5 cm box range (Figure 9a–c) do not demonstrate any significant variations concerning the geometry of the trail, when compared with the on-site investigation (Figure 9d).

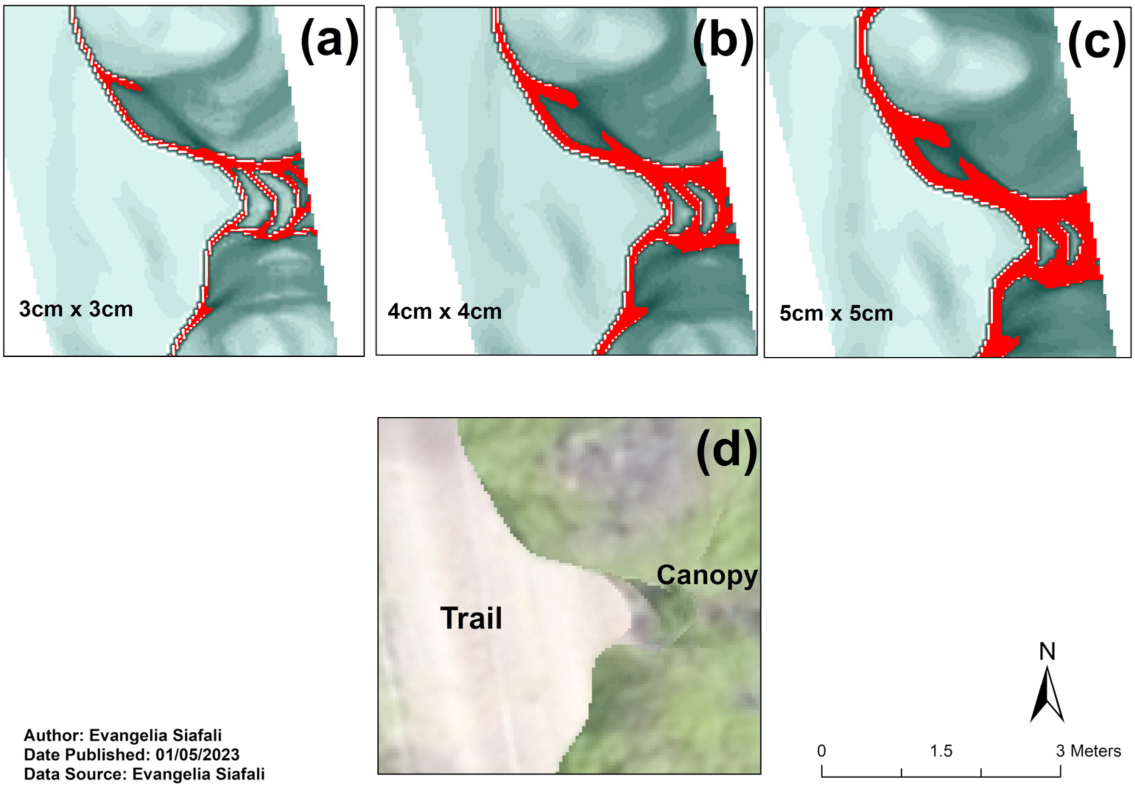

Figure 9. Earthworks calculation and distortion classification for: (**a**) 3 cm × 3 cm box range, (**b**) 4 cm × 4 cm box range, (**c**) 5 cm × 5 cm box range, and (**d**) trail geometry verified by on-site investigation (control).

The results of the earthworks calculations are displayed in Table 4. Values designated as 1 signify fill volume and values labeled as 2 indicate cut volume, whereas values over 55 cm are excluded and assigned the number 0. The pixel count was higher in fill volume than in cut volume. No considerable differences (52.98 m^3—4.26%) between the cut and fill volumes were evidenced.

Table 4. Cut and fill pixel count and area and volume calculations.

Value	Category	Pixel Count	Area (m^2)	Volume (m^3)
0	Excluded	20,842	833.68	208.42
1	Fill volume	129,666	5186.64	1296.66
2	Cut volume	124,368	4974.72	1243.68

We revisited our approach, utilizing the DEM for the precise detection of deformations exclusively on the forest trail surface, but this time with a higher classification precision of 0.001 cm, which resulted in the creation of 30 deformation classes. Figure 10 illustrates the deformations resulting from vehicular movement and tire-induced pressure (Figure 10a–c), as well as the visualization of water flow resulting from rainfall (Figure 10d–f).

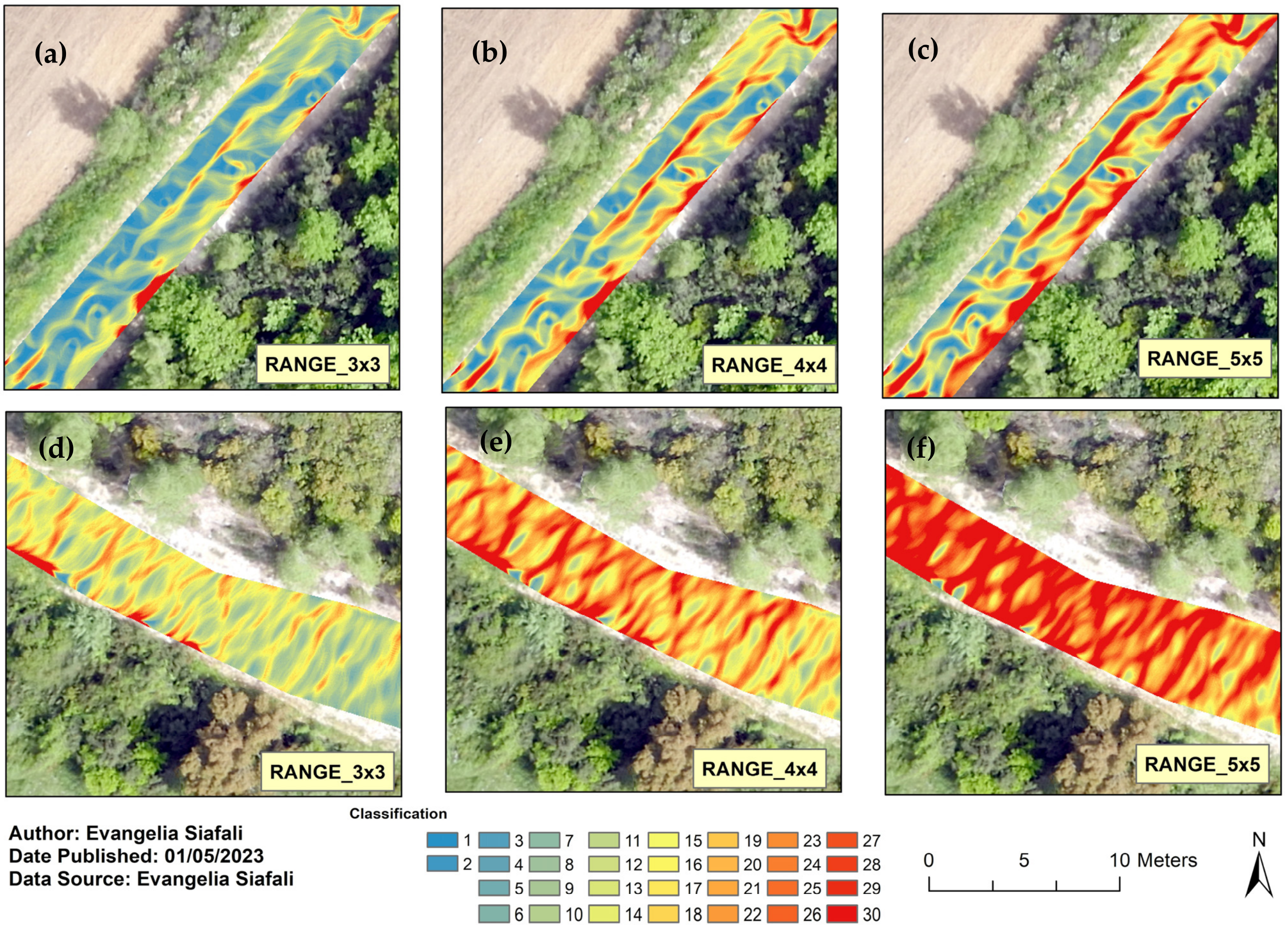

Figure 10. Visualization of 30 deformation classes from vehicular movement for: (**a**) range 3 cm × 3 cm box range, (**b**) 4 cm × 4 cm box range, and (**c**) 5 cm × 5 cm box range; and visualization of waterflow for: (**d**) 3 cm × 3 cm box range, (**e**) 4 cm × 4 cm box range, and (**f**) 5 cm × 5 cm box range.

3.5. Flood-Risk Map Generation

The collected data facilitated the generation of a comprehensive flood-risk map (Figure 11). It can serve as a valuable visualization tool when considering the implementation of infrastructure projects within various sections of the forest road networks, providing a nuanced understanding of the specific flood risks associated with these areas.

Based on the data analysis, it can be observed that the area mostly receives water from streams classified as fourth, third, and second, with a limited presence of first class streams. The deformations seen on the surface of the trail can be attributed to the shape of the hydrographic network and its distribution throughout the study area. In relation to the flood zone, a significant portion of the research area is classified under the categories of very low, low, and moderate. In summary, the region has a low index of susceptibility to flooding.

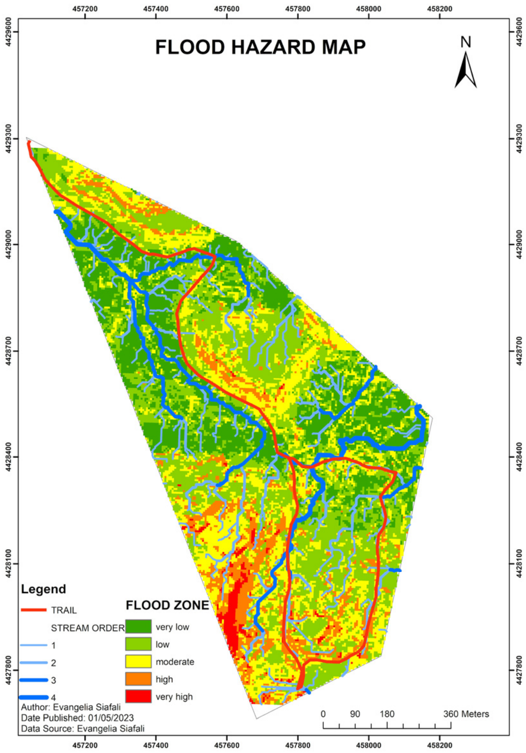

Figure 11. Flood hazard map of research area (Source: Siafali Evangelia 2023).

4. Discussion

In this study, we developed a novel approach for identifying and visualizing different types of surface deformation on a multi-use trail. This approach aims to enhance the quality of the trail, optimize its management, and obtain accurate data for performing technical operations and interventions on specific sections of the trail. A total of 20 and 30 altitude categories were established, each assigned specific ranges of values. The total area of each altitude group was calculated in square meters (m^2), and the volume of each category was measured in cubic meters (m^3). Furthermore, a Deformation Classification Model was developed for the examined trail, along with the calculation of earthworks and the creation of a flood-risk map. The aforementioned information will provide significant assistance to forest managers when constructing or maintaining trails and forest roads.

Our research bears some relevance with a previous study by Kim et al. [76], who used UAV photogrammetry technology to detect soil surface deformation in a timber harvest area. They reported that in order to have precise measurements with a polycopter UAV model, GCPs had to be established and a resolution < 3 cm was necessitated. However, in our case, precise measurements were possible in a much easier way, by utilizing a fixed-wing UAV equipped with the RTK function, which eliminates the need for setting GCPs or validation points.

Prior to the flight, our camera and UAV underwent automated calibration to ensure precise image capture with high precision. Unlike prior research [77–81], our objective did not include comparing raster files between pre-harvest and post-harvest. We conducted a study to examine the real-time deformations on the surface of the hybrid trail during the design phase or maintenance operations. To accomplish that, we compared the DSM and DEM reconstructed in Pix4DMapper, both obtained from the same flight.

In contrast to previous studies [76–79,82,83], which focused on relatively small areas, we conducted a comprehensive investigation of our model in a large-scale survey covering 149 hectares. The flight was conducted at 120 m height, as implemented in similar studies [76,80,82].

The DSM and the DEM that were generated were imported into ArcGIS Desktop to create the classification model. Further analysis in Pix4DMapper revealed that the mean, which represents the average inaccuracy in each of the three directions (X, Y, Z), was 0.000023 m, −0.000044 m, and 0.000177 m, respectively. The standard deviation of the error in each direction was 0.022535 m, 0.019567 m, and 0.020261 m. In addition, the RMS error was determined to be 0.022535 m, 0.019567 m, and 0.020262 m, respectively. The error values indicate a high level of accuracy, probably due to the precision of the Global Navigation Satellite System (GNSS) receiver used by the UAV and the camera's specifications. Our results are more accurate compared to the findings of Pierzchała et al. [80], who reported a spatial accuracy of the model with a total RMS error of 0.082 m and RMSEs of 0.056 m, 0.022 m, and 0.054 m for the X, Y, and Z dimensions, respectively.

In their study, Pierzchała et al. [80] observed that improved outcomes may be achieved by calibrating the camera and reducing the flying height to less than 155 m. The investigation conducted by Talbot et al. [84] demonstrated that flying at an altitude of 40–50 m above ground level resulted in a 2 cm spatial resolution orthomosaic. In contrast, Nevalainen et al. [82] managed to attain image resolutions of 2 and 3 cm by flying at altitudes of 100 and 150 m, respectively. Their study highlighted challenges faced by both human and UAV measurements in identifying the control surface level. In our case, we achieved comparable orthomosaic accuracy at a flight height of 120 m without encountering similar issues. This discrepancy could be attributed to the sparse vegetation along the surveyed trail and the utilization of more precise equipment in the current study.

Previous research has employed many techniques to detect rutting and deformations on the surfaces of skid trails and forest roads (e.g., [85–88]). In our work, we employed a novel approach that involved two distinct classifications based on the DSM and the DEM, both implemented using the same technique. Furthermore, we conducted an analysis on three raster cells measuring 3 cm × 3 cm, 4 cm × 4 cm, and 5 cm × 5 cm. The objective was to determine the optimal raster cell size based on the hybrid trail's surface topography. Such decision was supported by on-site investigations, considering the desired level of precision.

Determining the practicality of incorporating road surface deformations above specific thresholds, such as 5 cm, 6 cm, or 7 cm, is largely dependent on the outcomes of on-site investigations. These empirical assessments are crucial for validating the accuracy and relevance of the chosen pixel value thresholds in relation to the spatial resolution of the DEM employed in similar studies.

The Normalized Difference Vegetation Index (NDVI) can serve as a valuable tool for assessing the efficacy of management interventions and detecting variations in vegetation density along a given part of the forest road network. These data may be utilized to identify regions that may require maintenance or enhancement. Furthermore, this remote sensing technique also evaluates the impact of trail usage on nearby vegetation, detecting changes before and after road construction. The NDVI aids in designing trails to mitigate adverse effects on vegetation, showing lower values in areas with extensive trail usage, indicating reduced vegetation density, especially during drought seasons. Moreover, the generation of flood-risk maps is strongly suggested as a visualization tool of potential hazards. Stakeholders can use such maps to make informed decisions and implement measures that enhance the resilience of the infrastructure to potential flood events.

There were a total of 20 deformation categories based on the DSM and 30 deformation categories based on the DEM. Each category was allocated a certain range of values. The DSM classification was employed to detect significant distortions caused by the presence of trees, buildings, and steep slopes. The area of each altitude category was measured in square meters (m^2), while the volume of each category was quantified in cubic meters (m^3) to determine the volumes of excavation and filling. The DEM-based classification was utilized to accurately visualize the surface erosion of the hybrid trail and detect the flow of rainwater on it. This information, combined with the flood-risk map, allows for the prediction of erosion and facilitates the planning of maintenance activities and technical interventions in particular segments of the trail.

According to Latterini et al. [50], the effects of ground-based forest operations on forest soil must be studied beyond the physical impacts of machinery on the soil, which are frequently measured by eye inspection. Wood extraction systems, one of the more pronounced factors causing forest terrain deformation, should be studied to understand their impact on vegetation biodiversity, taking into consideration the regeneration of trees, shrubs, and plants. Our approach could assist similar research by offering fast and accurate information at a large scale on terrain deformation classes and identifying areas of special interest requiring further examination. One limitation of the present study is its focus in a specific area that is partially forested, which underlines the need for additional testing in various environmental scenarios. Our long-term aim is to integrate our approach as a valuable component in collaborative projects, fostering joint efforts to address broader environmental challenges.

5. Conclusions

This study introduces an innovative method for identifying deformations in the unpaved surfaces of trails and forest roads through the utilization of Unmanned Aerial Vehicles (UAVs) and high-precision spatial analysis. The information from the three-dimensional models derived from UAV data and LiDAR technology can assist forest managers in making more targeted decisions on road repair and maintenance, without expensive procedures and smart forest road structure monitoring in the future. Considering that terrestrial devices like GNSSs and terrestrial laser scanners are impractical in forested areas, the examined combination of a fixed-wing UAV with the RTK technology seems to provide an efficient alternative to achieve precise deformation monitoring of trails with centimeter-level precision. This approach concurrently diminishes labor-intensive efforts and could be widely implemented in situations when the objective is to effectively open up, monitor, maintain, and expand often complex forest road networks. The proposed methodology can also contribute to forest research by enabling large-scale and accurate data collection, thereby overcoming limitations associated with research costs.

The methodology presented in this study is characterized by its adaptability, ease of implementation, and cost-effectiveness, especially in the case of larger areas. In general, the selection of the most suitable technology for similar purposes is dependent on the particular aim and objectives of the data-gathering process since these technologies offer distinct spatial analytic capabilities, financial considerations, and operational needs. Future research endeavors should concentrate on further enhancing both precision and efficiency, particularly from an economic perspective, possibly by incorporating AI technologies.

Author Contributions: Conceptualization, E.S.; methodology, E.S.; software, E.S.; validation, E.S.; formal analysis, E.S.; investigation, E.S.; writing—original draft preparation, E.S. and P.A.T.; writing—review and editing, E.S. and P.A.T.; visualization, E.S. and P.A.T.; supervision, E.S. All authors have read and agreed to the published version of the manuscript.

Funding: This research received no external funding.

Data Availability Statement: Data are contained within the article.

Conflicts of Interest: The authors declare no conflicts of interest.

References

1. Kweon, H.; Seo, J.I.; Lee, J.-W. Assessing the Applicability of Mobile Laser Scanning for Mapping Forest Roads in the Republic of Korea. *Remote Sens.* **2020**, *12*, 1502. [CrossRef]
2. Dadrasjavan, F.; Zarrinpanjeh, N.; Ameri, A.; Engineering, G.; Branch, Q. Automatic Crack Detection of Road Pavement Based on Aerial UAV Imagery. *Preprints* **2019**, 2019070009. [CrossRef]
3. Lyons, C.K.; Borz, S.A.; Harvey, C.; Ramantswana, M.; Sakai, H.; Visser, R. Forest roads: Regional perspectives from around the world. *Int. J. For. Eng.* **2023**, *34*, 190–203. [CrossRef]
4. Tan, Y.; Li, Y. UAV photogrammetry-based 3D road distress detection. *ISPRS Int. J. Geo-Inf.* **2019**, *8*, 409. [CrossRef]
5. Xu, Q.; Li, M.; Jiang, X.; Zhang, Z.; Jiao, J.; Jian, J.; Li, J.; Yan, X.; Liang, Y.; Chen, T.; et al. Response of rill erosion to rainfall types and maintenance on the Loess Plateau: Implications for road erosion control. *Catena* **2022**, *219*, 106642. [CrossRef]
6. Marchi, W.; Visser, R.; Abbas, D.; Nordfjell, T.; Mederski, P.S.; Chung, W. Sustainable Forest Operations (SFO): A new paradigm in a changing world and climate. *Sci. Total Environ.* **2018**, *634*, 1385–1397. [CrossRef] [PubMed]

7. Picchio, F.; Latterini, F.; Mederski, P.S.; Tocci, D.; Venanzi, R.; Stefanoni, W.; Pari, L. Applications of GIS-based software to improve the sustainability of a forwarding operation in central Italy. *Sustainability* **2020**, *12*, 5716. [CrossRef]
8. Karagiannis, E. *Evaluation of Road Opening up in Greek Forests*; Scientific Yearbook; Department of Forestry and Natural Environmen, Aristotle University of Thessaloniki: Thessaloniki, Greece, 2008; pp. 714–727.
9. Dowling, R.; Newsome, D.; Moore, S. *Natural Area Tourism: Ecology: Impacts and Management*; Channel View Publications: Bristol, UK, 2013.
10. Santos, T.; Mendes, R.N.; Vasco, A. Recreational activities in urban parks: Spatial interactions among users. *J. Outdoor Recreat. Tourism* **2016**, *15*, 1–9. [CrossRef]
11. Wilkes-Allemann, J.; Ludvig, A.; Gobs, S.; Lieberherr, E.; Hogl, K.; Selter, A. Getting a grip on negotiation processes: Addressing trade-offs in mountain biking in Austria, Germany and Switzerland. *For. Pol. Econ.* **2022**, *136*, 102683. [CrossRef]
12. Wu, C.-C.; Li, C.-W.; Wang, W.-C. Low-impact hiking in natural areas: A study of nature park hikers' negative impacts and on-site leave-no-trace educational program in Taiwan. *Environ. Impact Assess. Rev.* **2021**, *87*, 106544. [CrossRef]
13. Wolf, I.D.; Wohlfart, T.; Brown, G.; Bartolomé Lasa, A. The use of public participation GIS (PPGIS) for park visitor management: A case study of mountain biking. *Tour. Manag.* **2015**, *51*, 112–130. [CrossRef]
14. Bíl, M.; Bílová, M.; Kubeček, J. Unified GIS database on cycle tourism infrastructure. *Tour. Manag.* **2012**, *33*, 1554–1561. [CrossRef]
15. Campelo, M.B.; Mendes, R.M.N. Comparing webshare services to assess mountain bike use in protected areas. *J. Outdoor Recreat. Tour.* **2016**, *15*, 82–88. [CrossRef]
16. Hagen, S.; Boyes, M. Affective ride experiences on mountain bike terrain. *J. Outdoor Recreat. Tour.* **2016**, *15*, 89–98. [CrossRef]
17. Nyelele, C.; Keske, C.; Chung, M.G.; Guo, H.; Egoh, B.N. Using social media data and machine learning to map recreational ecosystem services. *Ecol. Indic.* **2023**, *154*, 110606. [CrossRef]
18. Siebert, S.; Herden, J.; Gey, H. Self-assessment of riding skills and perception of trail difficulty in mountain biking—An investigation within the German-speaking mountain biking community. *J. Outdoor Recreat. Tour.* **2022**, *39*, 100500. [CrossRef]
19. Siafali, E. Implementation of Innovative Technologies in Surveying, Projecting, and Managing Hiking Trails. Ph.D. Thesis, Aristotle University of Thessaloniki, Thessaloniki, Greece, 2023.
20. Leung, Y.F.; Newburger, T.; Jones, M.; Kuhn, B.; Woiderski, B. Developing a monitoring protocol for visitor-created informal trails in Yosemite National Park, USA. *Environ. Manag.* **2011**, *47*, 93–106. [CrossRef]
21. Marion, Y.F.; Eagleston, H.; Burroughs, K.J.L. A review and synthesis of recreation ecology research findings on visitor impacts to wilderness and protected natural areas. *J. For.* **2016**, *114*, 352–362. [CrossRef]
22. Ramos-Scharrón, C.E.; Alicea-Díaz, E.E.; Figueroa-Sánchez, Y.A.; Viqueira-Ríos, R. Road cutslope erosion and control treatments in an actively-cultivated tropical montane setting. *Catena* **2022**, *209*, 105814. [CrossRef]
23. Ballantyne, M.; Pickering, C.M. Differences in the impacts of formal and informal recreational trails on urban forest loss and tree structure. *J. Environ. Manag.* **2015**, *159*, 94–105. [CrossRef]
24. Curran, M.P.; Murray, M.P. Soil disturbance, amelioration and rehabilitation affect forest growth, health, soil carbon and chemistry on five long-term soil productivity (LTSP) sites in southeastern British Columbia. *For. Ecol. Manag.* **2023**, *546*, 121362. [CrossRef]
25. Hammitt, W.E.; Cole, D.N.; Monz, C.A. *Wildland Recreation: Ecology and Management*, 2nd ed.; Wiley Blackwell: Chichester, UK, 1998.
26. Jamaluddin, J.; Kamarudin, N.; Ismail, M.H.; Ahmad, S.A. Optimizing timber transportation planning for timber harvesting using bees algorithm in Malaysia. *J. Environ. Manag.* **2023**, *340*, 117977. [CrossRef] [PubMed]
27. Lee, E.; Li, Q.; Eu, S.; Han, S.K.; Im, S. Assessing the impacts of log extraction by typical small shovel logging system on soil physical and hydrological properties in the Republic of Korea. *Heliyon* **2020**, *6*, e03544. [CrossRef]
28. Leung, J.L.; Marion, Y.F. Recreation impacts and management in wilderness: A state-of-knowledge review. *USDA For. Serv. Proc.* **2000**, *5*, 23–40.
29. Liddle, M. Recreation Ecology; Springer Dordrecht, The Netherlands, 1997.
30. Monz, C.A.; Marion, J.L.; Goonan, K.A.; Manning, R.E.; Wimpey, J.; Carr, C. Assessment and monitoring of recreation impacts and resource conditions on mountain summits: Examples from the Northern Forest, USA. *Mt. Res. Dev.* **2010**, *30*, 332–343. [CrossRef]
31. Naghdi, R.; Solgi, A.; Ilstedt, U. Soil chemical and physical properties after skidding by rubber-tired skidder in Hyrcanian forest, Iran. *Geoderma* **2016**, *265*, 12–18. [CrossRef]
32. Sahani, N.; Ghosh, T. GIS-based spatial prediction of recreational trail susceptibility in protected area of Sikkim Himalaya using logistic regression, decision tree and random forest model. *Ecol. Inf.* **2021**, *64*, 101352. [CrossRef]
33. Sitzia, T.; Rizzi, A.; Cattaneo, D.; Semenzato, P. Designing recreational trails in a forest dune habitat using least-cost path analysis at the resolution of visitor sight distance. *Urban For. Urban Green.* **2014**, *13*. [CrossRef]
34. Solgi, A.; Najafi, A.; Page-Dumroese, D.S.; Zenner, E.K. Assessment of topsoil disturbance caused by different skidding machine types beyond the margins of the machine operating trail. *Geoderma* **2020**, *367*, 114238. [CrossRef]
35. Deluca, T.H.; Freimund, W.A.; Cole, D.N. Influence of llamas, horses and hikers on soil erosion from established recreational trails in Western Montana, USA. *Environ. Manag.* **1998**, *22*, 255–262. [CrossRef]
36. Rickard, C.A.; McLachlan, A.; Kerley, G.I.H. The effects of vehicular and pedestrian traffic on dune vegetation in South Africa. *Ocean Coast. Manag.* **1994**, *23*, 225–247. [CrossRef]
37. Ballantyne, M.; Treby, D.L.; Quarmby, J.; Pickering, C.M. Comparing the impacts of different types of recreational trails on grey box grassy-woodland vegetation: Lessons for conservation and management. *Aust. J. Bot.* **2016**, *64*, 246–259. [CrossRef]

38. Cole, D.N.; Bayfield, N.G. Recreational trampling of vegetation: Standard experimental procedures. *Biol. Conserv.* **1993**, *63*, 209–215. [CrossRef]
39. Kutiel, P.; Eden, E.; Zhevelev, Y. Effect of experimental trampling and off-road motorcycle traffic on soil and vegetation of stabilised coastal dunes, Israel. *Environ. Conserv.* **2000**, *27*, 14–23. [CrossRef]
40. Lemauviel, S.; Rozé, F. Response of three plant communities to trampling in a sand dune system in Brittany (France). *Environ. Manag.* **2003**, *31*, 227–235. [CrossRef] [PubMed]
41. Young, R.A.; Gilmore, A.R. Effects of Various Camping Intensities on Soil Properties in Illinois Campgrounds. *Soil Sci. Soc. Am. J.* **1976**, *40*, 908–911. [CrossRef]
42. Akgul, M.; Yurtseven, H.; Akburak, S.; Demir, M.; Cigizoglu, H.K.; Ozturk, T.; Eksi, M.; Akay, A.O. Short term moniterning of forest road pavement degradation using terrestrial laser scanning. *Measurement* **2017**, *103*, 283–293. [CrossRef]
43. Mercier, P.; Aas, G.; Dengler, J. Effects of skid trails on understory vegetation in forests: A case study from Northern Bavaria (Germany). *For. Ecol. Manag.* **2019**, *453*, 117579. [CrossRef]
44. Olive, N.D.; Marion, J.L. The influence of use-related, environmental, and managerial factors on soil loss from recreational trails. *J. Environ. Manag.* **2009**, *90*, 1483–1493. [CrossRef]
45. Ganatsios, H.P.; Tsioras, P.A.; Papaioannou, A.G.; Blinn, C.R. Short Term Impacts of Harvesting 0perations on Soil Chemical Properties in a Mediterranean Oak Ecosystem. *Croat. J. For. Eng.* **2021**, *42*, 463–476. [CrossRef]
46. Jourgholami, M.; Hansson, L.J.; Högbom, L.; Jourgholami, M.; Laschi, A. Strategies to Mitigate the Effects of Soil Physical Disturbances Caused by Forest Machinery: A Comprehensive Review. *Curr. For. Rep.* **2022**, *8*, 20–37.
47. Marchi, R.; Spinelli, R.; Verani, S.; Venanzi, R.; Certini, G.E.; Picchio, R. Environmental impact assessment of different logging methods in pine forests thinning. *Ecol. Eng.* **2014**, *70*, 429–436. [CrossRef]
48. Solgi, A.; Lotfalian, M.; Rafiei, A.A.; Marchi, E.; Ilstedt, U. Combined effects of traffic intensity, skid trail slope, skidder type, and soil moisture content on soil degradation in the Hyrcanian forest of Iran. *Int. J. For. Eng.* **2023**, *34*, 385–396. [CrossRef]
49. Sadeghi, S.; Solgi, A.; Tsioras, P.A. Effects of traffic intensity and travel speed on forest soil disturbance at different soil moisture conditions. *Int. J. For. Eng.* **2022**, *33*, 146–154. [CrossRef]
50. Latterini, F.; Spinelli, R.; Venanzi, R.; Picchio, R. Acorn Review: Focus on ground-based extraction systems: Is skidding really more impactful than forwarding? *For. Ecol. Manag.* **2024**, *551*, 121514. [CrossRef]
51. Picchio, R.; Mederski, P.S.; Tavankar, F. How and How Much, Do Harvesting Activities Affect Forest Soil, Regeneration and Stands? *Curr. For. Rep.* **2020**, *6*, 115–128. [CrossRef]
52. Galidaki, G.; Zianis, D.; Gitas, I.; Radoglou, K.; Karathanassi, V.; Tsakiri–Strati, M.; Woodhouse, I.; Mallinis, G. Vegetation biomass estimation with remote sensing: Focus on forest and other wooded land over the Mediterranean ecosystem. *Int. J. Remote Sens.* **2017**, *38*, 1940–1966. [CrossRef]
53. Kweon, H. Comparisons of Estimated Circuity Factor of Forest Roads with Different Vertical Heights in Mountainous Areas, Republic of Korea. *Forests* **2019**, *10*, 1147. [CrossRef]
54. Mikita, T.; Krausková, D.; Hrůza, P.; Cibulka, M.; Patočka, Z. Forest Road Wearing Course Damage Assessment Possibilities with Different Types of Laser Scanning Methods including New iPhone LiDAR Scanning Apps. *Forests* **2022**, *13*, 1763. [CrossRef]
55. Talbot, B.; Astrup, R. A review of sensors, sensor-platforms and methods used in 3D modelling of soil displacement after timber harvesting. *Croat. J. For. Eng.* **2021**, *42*, 149–164. [CrossRef]
56. Šašak, J.; Gallay, M.; Kaňuk, J.; Hofierka, J.; Minár, J. Combined Use of Terrestrial Laser Scanning and UAV Photogrammetry in Mapping Alpine Terrain. *Remote Sens.* **2019**, *11*, 2154. [CrossRef]
57. Tomljanović, K.; Kolar, A.; Ðuka, A.; Franjević, M.; Jurjević, L.; Matak, I.; Ugarković, D.; Balenović, I. Application of UAS for Monitoring of Forest Ecosystems—A Review of Experience and Knowledge. *Croat. J. For. Eng.* **2022**, *43*, 487–504. [CrossRef]
58. Aldea, S.E.; Le Hégarat-Mascle, S. Robust crack detection for unmanned aerial vehicles inspection in an 409 a-contrario decision framework. *J. Electron. Imaging* **2015**, *24*, 061119. [CrossRef]
59. Grandsaert, P.J. *Integrating Pavement Crack Detection and Analysis Using Autonomous Unmanned Aerial Vehicle Imagery*; Air Force Institute of Technology: Wright-Patterson, OH, USA, 2015.
60. Sankarasrinivasan, S.; Balasubramanian, E.; Karthik, K.; Chandrasekar, U.; Gupta, R.S. Health Monitoring of Civil Structures with Integrated UAV and Image Processing System. *Procedia Comput. Sci.* **2015**, *54*, 508–515. [CrossRef]
61. Alfio, V.S.; Costantino, D.; Pepe, M. Influence of Image TIFF Format and JPEG Compression Level in the Accuracy of the 3D Model and Quality of the Orthophoto in UAV Photogrammetry. *J. Imaging* **2020**, *6*, 30. [CrossRef] [PubMed]
62. Anifantis, A.S.; Camposeo, S.; Vivaldi, G.A.; Santoro, F.; Pascuzzi, S. Comparison of UAV Photogrammetry and 3D Modeling Techniques with Other Currently Used Methods for Estimation of the Tree Row Volume of a Super-High-Density Olive Orchard. *Agriculture* **2019**, *9*, 233. [CrossRef]
63. Manajitprasert, S.; Tripathi, N.K.; Arunplod, S. Three-Dimensional (3D) Modeling of Cultural Heritage Site Using UAV Imagery: A Case Study of the Pagodas in Wat Maha That, Thailand. *Appl. Sci.* **2019**, *9*, 3640. [CrossRef]
64. Pourreza, M.; Moradi, F.; Khosravi, M.; Deljouei, A.; Vanderhoof, M.K. GCPs-Free Photogrammetry for Estimating Tree Height and Crown Diameter in Arizona Cypress Plantation Using UAV-Mounted GNSS RTK. *Forests* **2022**, *13*, 1905. [CrossRef]
65. Tomaštík, J.; Mokroš, M.; Surový, P.; Grznárová, A.; Merganič, J. UAV RTK/PPK Method—An Optimal Solution for Mapping Inaccessible Forested Areas? *Remote Sens.* **2019**, *11*, 721. [CrossRef]

66. Nakagomi, H.; Fuse, Y.; Nagata, Y.; Hosaka, H.; Miyamoto, H.; Yokozuka, M.; Kamimura, A.; Watanabe, H.; Tanzawa, T.; Kotani, S. Forest road surface detection using LiDAR-SLAM and U-Net. In Proceedings of the 2021 IEEE/SICE International Symposium on System Integration, SII 2021, Online, 11–14 January 2021; pp. 727–732.
67. Luetzenburg, G.; Kroon, A.; Bjørk, A.A. Evaluation of the Apple iPhone 12 Pro LiDAR for an Application in Geosciences. *Sci. Rep.* **2021**, *11*, 22221. [CrossRef]
68. Zeybek, B.M.; Biçici, S. Road Distress Measurements Using UAV. *Turk. J. Remote Sens. GIS* **2020**, *1*, 13–23.
69. Baiocchi, V.; Del Pizzo, S.; Monti, F.; Pugliano, G.; Onori, M.; Robustelli, U.; Troisi, S.; Vatore, F.; León Trujillo, F.J. Solutions and limitations of the geomatic survey of an archaeological site in hard to access areas with a latest generation smartphone: The example of the Intihuatana stone in Machu Picchu (Peru). *ACTA IMEKO* **2022**, *11*, 8. [CrossRef]
70. Díaz-Vilariño, L.; Tran, H.; Frías, E.; Balado, J.; Khoshelham, K. 3D mapping of indoor and outdoor environments using Apple smart devices. *Int. Arch. Photogramm. Remote Sens. Spatial Inf. Sci.* **2022**, *XLIII-B4-2022*, 303–308.
71. Zhu, L.; Zhang, H.; Li, X.; Zhu, F.; Liu, Y. GNSS Timing Performance Assessment and Results Analysis. *Sensors* **2022**, *22*, 2486. [CrossRef] [PubMed]
72. Hruza, T.; Tyagur, N.; Krejza, Z.; Cibulka, M.; Procházková, A.; Patocka, Z.P. Detecting Forest Road Wearing Course Damage Using Different Methods of Remote Sensing. *Remote Sens.* **2018**, *10*, 492. [CrossRef]
73. Zagas, T.; Karagiannis, E.; Zagka, T.; Siafali, E. Investigation for the signage of the Mavrobara hiking trail in Polichrono Halkidiki. 2018.
74. Strahler, A.N. Quantitative analysis of watershed geomorphology. *Eos Trans. AGU* **1957**, *38*, 913–920.
75. European Ramblers' Association. Available online: https://www.era-ewv-ferp.org/ (accessed on 28 October 2023).
76. Kim, J.; Kim, I.; Ha, E.; Choi, B. UAV Photogrammetry for Soil Surface Deformation Detection in a Timber Harvesting Area, South Korea. *Forests* **2023**, *14*, 980. [CrossRef]
77. Marra, E.; Cambi, M.; Fernandez-Lacruz, R.; Giannetti, F.; Marchi, E.; Nordfjell, T. Photogrammetric estimation of wheel rut dimensions and soil compaction after increasing numbers of forwarder passes. *Scand. J. For. Res.* **2018**, *33*, 613–620. [CrossRef]
78. Marra, E.; Laschi, A.; Fabiano, F.; Foderi, C.; Neri, F.; Mastrolonardo, G.; Nordfjell, T.; Marchi, E. Impacts of wood extraction on soil: Assessing rutting and soil compaction caused by skidding and forwarding by means of traditional and innovative methods. *Eur. J. For. Res.* **2022**, *141*, 71–86. [CrossRef]
79. Cambi, M.; Giannetti, F.; Bottalico, F.; Travaglini, D.; Nordfjell, T.; Chirici, G.; Marchi, E. Estimating machine impact on strip roads via close-range photogrammetry and soil parameters: A case study in central Italy. *IForest* **2018**, *11*, 148–154. [CrossRef]
80. Pierzchała, M.; Talbot, B.; Astrup, R. Estimating Soil Displacement from Timber Extraction Trails in Steep Terrain: Application of an unmanned aircraft for 3D Modelling. *Forests* **2014**, *5*, 1212–1223. [CrossRef]
81. Howell, R.; Aust, W.M.; Bolding, M.C. Forestry best management practices and modeled erosion on planned and logger-selected bladed skid trails in the Ridge and Valley region, Virginia, USA. *Int. J. For. Eng.* **2019**, *30*, 68–75. [CrossRef]
82. Nevalainen, P.; Salmivaara, A.; Ala-Ilomäki, J.; Launiainen, S.; Hiedanpää, J.; Finér, L.; Pahikkala, T.; Heikkonen, J. Estimating the rut depth by UAV photogrammetry. *Remote Sens.* **2017**, *9*, 1279. [CrossRef]
83. Pierzchała, M.; Talbot, B.; Astrup, R. Measuring wheel ruts with close-range photogrammetry. *Forestry* **2016**, *89*, 383–391. [CrossRef]
84. Talbot, B.; Rahlf, J.; Astrup, R. An operational UAV-based approach for stand-level assessment of soil disturbance after forest harvesting. *Scand. J. For. Res.* **2018**, *33*, 387–396. [CrossRef]
85. Lee, E.; Eu, S.; Li, Q. Assessment of Soil Erosion Potential from the Disturbed Surface of Skid Trails in Small Shovel Harvesting System. *Front. Environ. Sci.* **2022**, *10*, 756848. [CrossRef]
86. Botha, T.; Johnson, D.; Els, S.; Shoop, S. Real time rut profile measurement in varying terrain types using digital image correlation. *J. Terramech.* **2019**, *82*, 53–61. [CrossRef]
87. Aricak, B. Using remote sensing data to predict road fill areas and areas affected by fill erosion with planned forest road construction: A case study in Kastamonu Regional Forest Directorate (Turkey). *Environ. Monit. Assess.* **2015**, *187*, 417. [CrossRef]
88. Ćwiąkała, P.; Kocierz, R.; Puniach, E.; Nędzka, M.; Mamczarz, K.; Niewiem, W.; Wiącek, P. Assessment of the possibility of using Unmanned Aerial Vehicles (UAVs) for the documentation of hiking trails in alpine areas. *Sensors* **2018**, *18*, 81. [CrossRef]